
TARGO: Benchmarking Target-driven Object Grasping under Occlusions

Yan Xia^{1,4*} Ran Ding^{1*} Ziyuan Qin^{1*} Guanqi Zhan³
Kaichen Zhou³ Long Yang² Hao Dong² Daniel Cremers^{1,4}
¹Technical University of Munich ²CFCS, School of CS, Peking University
³University of Oxford ⁴Munich Center for Machine Learning (MCML)

Abstract

Recent advances in predicting 6D grasp poses from a single depth image have led to promising performance in robotic grasping. However, previous grasping models face challenges in cluttered environments where nearby objects impact the target object’s grasp. In this paper, we first establish a new benchmark dataset for TARget-driven Grasping under Occlusions, named TARGO. We make the following contributions: 1) We are the first to study the occlusion level of grasping. 2) We set up an evaluation benchmark consisting of large-scale synthetic data and part of real-world data, and we evaluated five grasp models and found that even the current SOTA model suffers when the occlusion level increases, leaving grasping under occlusion still a challenge. 3) We also generate a large-scale training dataset via a scalable pipeline, which can be used to boost the performance of grasping under occlusion and generalized to the real world. 4) We further propose a transformer-based grasping model involving a shape completion module, termed TARGO-Net, which performs most robustly as occlusion increases. Our benchmark dataset can be found at <https://TARGO-benchmark.github.io/>.

1 Introduction

Grasping in cluttered environments is a challenging and fundamental task in robotics and computer vision, which always requires a robot to analyze the geometry and physical properties of objects from a partial point cloud captured by a single depth camera and determine robust poses for grasping with a parallel-jaw gripper. Recent years have witnessed significant advancements in this field, fueled by the development of algorithms [15, 1, 55] that predict the 6D grasp poses of objects from depth observations and the availability of large-scale simulation and real-world datasets [14, 23, 7, 8]. However, the robustness of target-oriented grasp models in real-world applications, particularly in the presence of varying occlusion levels, has not been explored [25, 28]. The scanned data from depth cameras are often incomplete and noisy owing to natural occlusion or self-occlusion.

To study the occlusion problem, in this paper, we propose a new benchmark, TARGO, to analyze the robustness of target-driven grasp models against occlusion. TARGO includes synthetic and real-world datasets named TARGO-Synthetic and TARGO-Real, respectively. TARGO-Synthetic is derived from VGN (BSD 3-Clause License) [1] and created by synthetically arranging multiple objects on a tabletop in a disorganized fashion. This dataset facilitates systematic analysis of occlusion effects in grasping by examining occluder properties such as severity and existence of occluder. Furthermore, we introduce real-world grasping data, TARGO-Real, which comprises real-world objects with natural occlusion. The objects in TARGO-Real are selected from the DexYCB dataset (license CC BY-NC 4.0) [3], with a total of 3,225 scenes, enabling validation of grasping trained in the synthetic environment within a real-world setting.

*Equal contribution.

We investigate the impact of occlusion on five previous SOTA models for the target-driven grasping task. We aim to assess the generalization capabilities of these models through extensive experiments when confronted with different occlusion levels within both synthetic and natural environments. Experimental results show that the current SOTA models have an apparent decrease in grasp success rate as the occlusion level increases.

Inspired by [9], data augmentation is a widely applied technique to solve the distribution shift problem. We find that incorporating single scenes where only the target object in a scene can increase the robustness of grasping models against occlusion. We then propose TARGO-Net, a transformer-based model for target-driven grasping against occlusion. Different from the previous grasp models with scene completion (e.g., GIGA[15]), our TARGO-Net employs more effective shape completion for robotic grasping. To validate its effectiveness, we extensively evaluate TARGO-Net on the proposed TARGO-Synthetic and TARGO-Real datasets, demonstrating its robustness in target-driven grasp under occlusion across both synthetic and natural environments.

In summary, we make the following contributions:

- To the best of our knowledge, we are the first to focus on the problem of target-driven grasping under occlusion.
- We set up a new benchmark dataset, TARGO, to study occlusion in target-driven robotic grasping task. TARGO consists of large-scale synthetic data for a systematic study and real-world objects with natural occlusions for zero-shot generalization.
- We propose an effective transformer-based grasping model, TARGO-Net, involving a 3D shape completion module. Extensive experiments in both simulation and real-world environments show it performs better than the state-of-the-art under occlusion.

2 Related Work

Grasping is a widely studied field in robotics. In the following, we first review the existing occlusion handling and target-oriented grasping methods in clutter, and then give a brief review of shape completion from point clouds.

Occlusion Handling. Both computer vision and robotics systems suffer from occlusion as it means lost of information at the perception side and obstacle at the manipulation side. Occlusion remains a challenge for different computer vision tasks, and there have been efforts trying to handle occlusion in various vision tasks, including object recognition [19, 29], object detection [35, 16], instance segmentation [47, 16, 49], tracking [10, 11, 38] and video action recognition [27]. Besides, another series of work study the occlusion problem itself, with the goal of reconstructing the complete shape of partially visible objects, *i.e.*, amodal segmentation [54, 51, 50, 43, 29]. Occlusion is also challenging for the robotics community, where the occlusion problem does matter in mapping [32, 53, 13], object retrieval [21], manipulation [37, 24], navigation [52, 6, 36], grasping [33, 48] or rearrangement [5, 22] in clutters. In our paper, we study the task of grasping in clutter, where we formulate the occlusion problem via a new benchmark and develop a new baseline to handle the occlusion problem more robustly.

Grasping in Clutter. The task of grasping in clutter requires avoiding collisions with obstacles, making grasp planning more complex. VGN [1] and GIGA [15] utilize 3D convolutional neural networks (CNNs) to predict grasp configurations for each voxel within the reconstructed truncated signed distance field (TSDF). In contrast, contact-based methods such as Edge Grasp Networks [12] and Contact GraspNet [33] directly infer the SE(3) pose, width, and grasp quality for individual points in the point cloud. Further, ICGNet [55] integrates the prediction of instance segmentation masks, collision-free grasp configurations, and object reconstructions from a single-view point cloud to achieve better accuracy. Target-driven grasping [28, 25, 44] specifies the target object for grasping. Under heavy occlusion, these methods typically first detect and remove all blocking objects before accessing the target. Our approach, however, directly grasps the target object without removing obstructing items. Our TARGO-Net segments and reconstructs the target object, then plans the optimal target grasp, enhancing both accuracy and efficiency in cluttered environments.

Shape Completion. Thanks to advances in deep learning and extensive 3D datasets, learning-based methods now achieve excellent performance in shape completion tasks. Several approaches [39, 26, 31] utilize volumetric representations of objects, enabling the application of 3D convolution to

learn complex topologies and tessellations. PCN [46] employs an encoder for feature extraction, producing a dense, completed point cloud from sparse inputs. TopNet [34] introduces a decoder with a hierarchical structure for point cloud generation based on a rooted tree. VPC-Net [41] is designed for vehicle point cloud completion using raw LiDAR scans. ASFM-Net [42] captures detailed shapes prior information to point cloud completion by mapping partial and complete input point clouds into a shared latent space. Recently, AdaPoinTr [45] implemented an adaptive query generation mechanism and introduced a novel denoising task. In addition, some researchers jointly explore predicting scene completion and robotic grasping due to their correlation. ShellGrasp-Net [4] predicts grasp affordances and entry/exit depth maps by jointly learning camera-ray intersections with isolated objects. Recent GIGA [15] advances grasp prediction and scene reconstruction in cluttered scenes by integrating VGN [1] and Convolutional Occupancy Networks [30]. Unlike scene completion, we employ AdaPoinTr for shape completion in robotic grasping in this study.

3 Benchmarking Occlusion in Grasping

To evaluate the robustness of current TARGET-driven Grasping under Occlusions, we introduce a new benchmark dataset named TARGO. TARGO covers cluttered scenarios with different occlusion levels, featuring both synthetic and real-world data. The synthetic dataset facilitates controlled occlusion studies and tests robotic grasping models under different occlusions. Additionally, we provide a real-world dataset comprising cluttered scenes with natural occlusions. This dataset provides an opportunity to examine the performance of models under more realistic objects.

3.1 Design Parameters

We investigate two key attributes of occlusion: the existence of occluder (single scene versus cluttered scene) and the levels of occlusion (the extent to which the target object is occluded). By analyzing these attributes, we aim to comprehensively understand the impact of occlusion on robotic grasping.

The existence of occluder. In our study, we aim to grasp the target among all the objects in a given cluttered scene captured by a single-view RGB-D camera. We thus define *occluder* as all the objects in the cluttered scene beside the target object and *single scene* as a scene with only the target object to grasp on the table. Note that the camera pose of the target in a single scene is the same as that in the corresponding cluttered scene. Based on these definitions, we have three types of grasps in single and cluttered scenes: 1) Grasps that would fail in both single and cluttered scenes due to the block of the supporting table or the limit of the max opening width of the parallel gripper. 2) Grasps that would succeed in single scenes but fail in cluttered scenes due to the blocking of occluders. 3) Grasps that would succeed in both single and cluttered scenes. Note that no grasp would succeed in cluttered scenes but fail in single scenes. Thus, the set of successful grasps in cluttered scenes is a subset of the set of successful grasps in single scenes. Therefore, sampling grasps from single scenes allows us to learn from see how the unoccluded target could be grasped and how occluders affect the target-driven grasping. To demonstrate the effectiveness of single scenes, we augment cluttered scenes with single scenes in Section 5.1.

Levels of occlusion. In our study, we consider a range of occlusion levels (OL) from 0-90%. We exclude cases where more than 90% of the target is occluded because the view is almost completely blocked, making the target hard to discern and of little practical concern. We quantify *occlusion level* as a visual obstruction of the target object in 2D depth images, defined as a simple division between the sum of unoccluded pixels in the partially observed target and n , the total number of pixels of the complete target:

$$OL = \frac{\sum_{i=1}^n \mathbb{1}_i}{n} \quad (1)$$

where $\mathbb{1}_i = 1$ if pixel i in the complete target is occluded, and 0 if not.

3.2 Benchmark Datasets

We present synthetic and real-world datasets to thoroughly investigate the occlusion challenge in robotic grasping. The synthetic dataset can be used to train and evaluate the target-driven grasping models under various occlusion levels, and the real-world one can be tested for zero-shot transfer to evaluate grasping performance in practice.

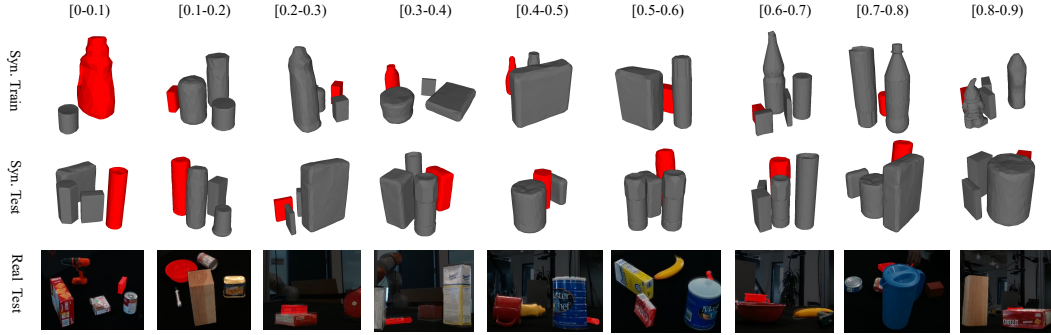


Figure 1: Examples of our TARGO-Synthetic training/test sets and TARGO-Real datasets with occlusion levels from $[0, 0.1)$ to $[0.8, 0.9)$. The red one is the target to grasp.

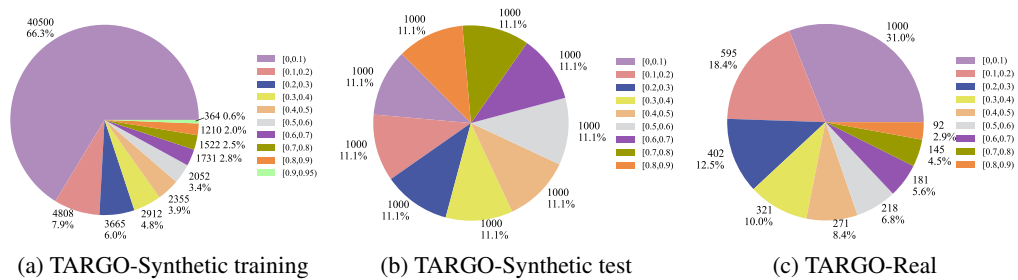


Figure 2: Target counts in our TARGO under different occlusion levels.

Table 1: Comparisons of publicly available grasp datasets. Grasp labels are generated either manually (✍), by physics simulation (🎯), analytical models (f), or real-world trials (👁).

Dataset	Labels	Observation	Type	Total Objects (Per Scene)	Total Grasps (Per Scene)	Modality	Occlusion
Cornell [14]	✍	Real	Rect.	240 (1)	8019 (~8)	RGB-D	\times
Levine et al. [23]	👁	Real	Rect.	- (-)	800k (1)	RGB-D	\times
GraspNet-1Billion [8]	f	Real	6-DoF	88 (~10)	~1.2B (3-9M)	RGB-D	\times
Acronym [7]	🎯	Sim	6-DoF	8872 (-)	17.7M (2000)	Depth	\times
VGN [1]	🎯	Sim	6-DoF	114 (~5)	~6M (120)	Depth	\times
TARGO (Ours)	🎯	Sim + Real	6-DoF	135 (~5)	~6M (~350)	Depth	\checkmark

Table 1 compares our TARGO with other publicly available grasp datasets. TARGO samples 6-DoF grasps from single scenes in addition to cluttered scenes for synthetic training and testing, employs 21 YCB objects [2] for real-world testing, and includes approximately 350 grasps per scene. Among these datasets, we are the only one to incorporate both simulation and real-world observations. By combining both simulation and real-world observations, we could quickly generate single scenes, use real-world inputs, and achieve a scalable pipeline with practical applications. More importantly, no existing datasets have considered occlusion effects. To the best of our knowledge, our work is the first to explore the impact of occlusion on robotic grasping. Fig. 1 shows examples of our simulation and real-world grasp data in various occlusion levels.

TARGO-Synthetic dataset. Our synthetic training dataset consists of 61,119 target objects distributed across 16,640 cluttered scenes, as shown in Fig. 2a. Each object in a cluttered scene is sampled as a target, so the number of single scenes matches the number of target objects. The dataset incorporates occlusions ranging from $[0, 0.1)$ to $[0.9, 0.95)$, divided into 10 occlusion level bins. As expected, the target count is highest for $OL \in [0, 0.1)$ due to our random placement strategy, which ensures that each object in the cluttered scenes is sampled as a target. In the test set, most clutter removal methods [1, 15, 12] conduct approximately 5 rounds of online experiments, with about 100 scenes in each round. This evaluation strategy is slow, inaccurate (low number of experiments), and mostly ignores high occlusion. However, to account for varying occlusion levels in target-driven grasping, we first generate 1,000 offline scenes for 9 occlusion level bins, from $[0, 0.1)$ to $[0.8, 0.9)$

(seen in Fig. 2b). By conducting numerous experiments and ensuring uniform trials at each occlusion level, we achieve a reliable grasp success rate that accounts for high occlusion scenarios. This generation and evaluation method could also be applied to other robotic tasks.

TARGO-Real dataset. This dataset focuses on real-world occlusions and consists of raw data captured by depth cameras, which exhibit various noise patterns, distinct occlusion configurations, and different object types and shapes from our simulation objects. The dataset comprises 21 DexYCB objects [3] selected from the YCB [2] dataset, totaling 3,225 scenes. Fig. 2c shows the target counts under different occlusion levels. The distribution under **natural occlusion** shows a similar trend to the TARGO-Synthetic training dataset: target counts in $OL \in [0, 0.1)$ occupy 31% of the total targets and gradually decrease for higher OL. The slight distinction of distribution between Fig. 2b and Fig. 2c stem from workspace size, test objects, human placement vs random placement, etc.

3.3 Target-driven Grasping Models

We study several existing robotic grasping models with diverse properties for this benchmark. We find that many existing grasping models [25, 28, 44] resort to removing visually blocking objects before grasping the target due to occlusion of closely surrounding undesired objects. However, our study aims to directly grasp the target. Thus, we adapt the clutter removal methods [1, 15, 12] to target-driven grasping in cluttered scenes as our baseline models. All employed models underwent fully supervised training on the training split of the synthetic dataset, and were then evaluated on TARGO-Synthetic test and zero-shot transferred to TARGO-Real to assess their practical grasping capability.

3.4 Evaluation Metric

Following [15, 1], we apply the grasp success rate (GSR) as our evaluation metric for target-driven grasping. Given N grasp trials, GSR can be defined as:

$$\text{GSR} = \frac{1}{N} \sum_{i=1}^N \mathbb{1}_i, \quad (2)$$

where $\mathbb{1}_i = 1$ if the i -th grasp is successful, and 0 if it fails.

3.5 Preliminary Benchmark Analysis

Fig. 4 shows performances of our TARGO-Net (to be introduced in Section 4) versus baseline methods. The plot clearly shows that all baseline methods exhibit an apparent decline in grasp success rate comparing values at occlusion level $[0, 0.1)$ and $[0.8, 0.9)$. EdgeGraspNet and its variant VN-EdgeGraspNet decline the most at high occlusion levels, with an absolute decline up to 30%. The reason is that their inputs include no scene information, and the local input patch does not guarantee collision-free grasps. VGN [1], GIGA, and its variant GIGA-HR [15] exhibit an approximate total decrease of 20%, as they all sample grasps exclusively in cluttered scenes, and both GIGA and GIGA-HR poorly reconstruct the target object. Overall, the lack of robustness against occlusion underscores the need for future studies to account for occlusion in robotic grasping.

4 Our TARGO-Net

4.1 Problem formulation

Given a cluttered scene point cloud $P \in \mathbb{R}^{N_s \times 3}$ consisting of K different objects captured by the depth camera, where N_s is the number of points, we first segment the target object P_k using a widely used segmentation model and then obtain the completed target point cloud P'_k utilizing a pre-trained 3D shape completion model. To predict a 6-DoF pose that successfully grasps the target and avoids collisions with occluders, we aim to learn the function: $F(P'_k, P) : \mathbf{t} \rightarrow q, \mathbf{r}, w$, where the grasp center $\mathbf{t} \in \mathbb{R}^3$ is mapped to grasp quality $q \in [0, 1]$, rotation $\mathbf{r} \in \text{SO}(3)$, and gripper width $w \in \mathbb{R}$.

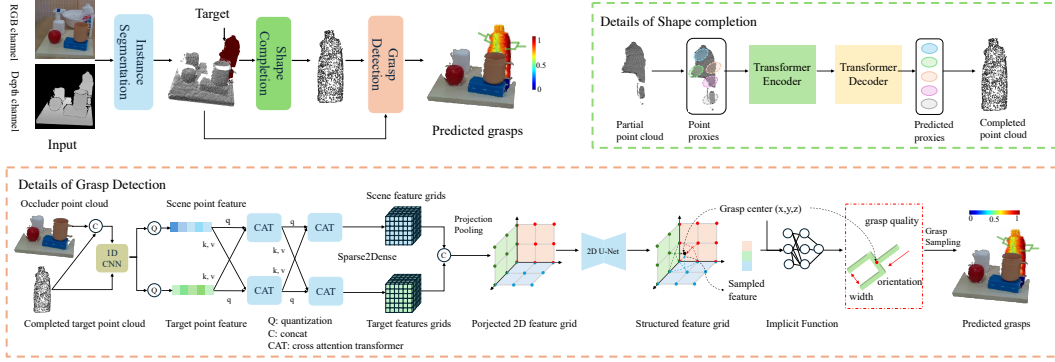


Figure 3: Model architecture of our TARGO-Net, consisting of instance segmentation, shape completion, and grasp detection modules. *Grasp detection.* We first concatenate the cluttered scene point cloud and the target point cloud, feeding them into a shared 1D CNN layer. Next, we quantize the scene and target point features separately. Using a Cross-Attention Transformer and Sparse2Dense operations, we obtain 3D feature grids, which are then projected, pooled, and processed using a 2D U-Net to obtain 2D feature grids. Finally, an affordance implicit function is applied to obtain 6-DoF grasps and the corresponding grasp quality. A sampling technique is employed to select and refine the optimal grasps.

4.2 Model Architecture

Fig. 3 shows our TARGO-Net pipeline. Given a noisy RGB-D image, we first segment the target object from the scene. Next, we feed the partial target point cloud into a shape completion network, outputting a completed target point cloud. After combining the target point cloud and the scene point cloud, we aim to predict the grasp quality, rotation, and width field using a designed affordance prediction network, from which potential 6-DoF grasps can be sampled.

4.2.1 3D Instance Segmentation

Given an RGB-D image capture by a real sense camera, we utilize SAM [18] alongside a visual prompt to segment the target object from the scene. Subsequently, we back-project the depth maps to generate point clouds, obtaining the partial target and the scene point clouds. The partial target point cloud is then fed into our shape completion network.

4.2.2 3D Shape Completion

Following AdaPoinTr [45], we construct our 3D shape completion model, as shown in Fig. 3 (top right). First, we convert the input partial point cloud to a sequence of point proxies, a set of feature vectors representing local regions. Then, we utilize the geometry-aware Transformer to take the point proxies and predict the point proxies of missing points. Finally, the missing point cloud is predicted based on the output point proxies. Note that in our study, we need no additional datasets to train the shape completion network since every target object in a single scene has the corresponding ground-truth complete point cloud in our TARGO-Synthetic dataset.

4.2.3 Grasp Detection Network

Fig. 3 shows our grasp detection network architecture, consisting of the sparse feature encoder, implicit function decoder, and grasping sampling modules.

Sparse feature encoder. We first process the scene point cloud and the completed target object point cloud through a shared 1D CNN layer, extracting point features for both the scene and the target object. We then quantize these point features to create sparse features for the scene and target, respectively. To improve the target and scene relationship modeling, we further incorporate a cross-attention fusion module with two parallel Cross-Attention Transformers (CAT) inspired by CASSPR [40]. In the first CAT, a multi-head cross-attention layer uses the sparse scene features as the query and the sparse target features as the key and value. Conversely, the second CAT operates the sparse target features as the query and the sparse scene features as the key and value. With the

cross-attention fusion, both the scene and target point cloud features are enhanced by considering the contextual relationship between the target object and the clutter scene.

Implicit function decoder. Next, we convert the enhanced sparse features to produce the dense scene grid features and target grid features and then concatenate them. Following GIGA [15], we use orthogonal projection and average pooling to generate three planar features. A 2D-UNet processes these planar features, which are then concatenated into a single feature. Finally, three implicit decoders, utilizing the position and processed features, predict the implicit fields of grasp quality, rotation, and width.

Grasp sampling. We develop a grasp sampling strategy to identify successful grasps within a defined workspace: a 0.3 m^3 cube divided into a grid of $40 \times 40 \times 40$ cells. The center of each cell within the grid serves as a query point for the implicit field, resulting in a set of 64,000 points that act as the centers for potential grasps. These query points are processed by the implicit field to generate output voxels: quality voxels, rotation voxels, and width voxels. To refine the grasp sampling process, we preprocess the quality voxels using the TSDF (Truncated Signed Distance Function) grid of the completed target object as a reference. Smoothing techniques are employed to enhance data quality and focus on near-surface external areas as regions of interest for potential grasps. Additionally, Non-Maximum Suppression (NMS) is applied to select the most probable grasp centers. From these selected centers, we determine the grasp poses and their corresponding rotations.

4.3 Loss Functions

Following the same training objective as VGN [1], TARGO-Net is trained end-to-end on simulated ground-truth grasps with the loss function:

$$\mathcal{L}(\hat{g}, g) = \mathcal{L}_q(\hat{q}, q) + q(\mathcal{L}_r(\hat{\mathbf{r}}, \mathbf{r}) + \mathcal{L}_w(\hat{w}, w)), \quad (3)$$

where \mathcal{L}_q is a binary cross-entropy loss that compares the predicted grasp quality \hat{q} with the ground truth q ; \mathcal{L}_w is the mean-squared error between the predicted and ground-truth gripper widths \hat{w} and w , respectively. For orientation, we use the inner product to compute the distance between the predicted quaternion $\hat{\mathbf{r}}$ and target quaternion \mathbf{r} : $\mathcal{L}_{quat}(\hat{\mathbf{r}}, \mathbf{r}) = 1 - |\hat{\mathbf{r}} \cdot \mathbf{r}|$ [20]. However, as parallel-jaw gripper is symmetric and a configuration rotated by 180° around the gripper’s wrist axis essentially corresponds to the same grasp, both mirrored rotations \mathbf{r} and \mathbf{r}_π are considered as ground truth. Therefore, the orientation loss is defined as:

$$\mathcal{L}_r(\hat{\mathbf{r}}, \mathbf{r}) = \min(\mathcal{L}_{quat}(\hat{\mathbf{r}}, \mathbf{r}), \mathcal{L}_{quat}(\hat{\mathbf{r}}, \mathbf{r}_\pi)). \quad (4)$$

Note that grasp orientation and gripper width are only supervised when a grasp is successful ($q = 1$).

5 Experiments

Training setup. We train our TARGO-Net for 15 epochs using Adam optimizer [17] with a learning rate of 2×10^{-4} and a batch size of 32. The training process takes approximately 5 days on an NVIDIA A40-48GB GPU.

Target-driven grasping results. We compare the performance of our method and the baselines on TARGO-Synthetic test: VGN [1], GIGA and GIGA-HR [15], EdgeGraspNet and VN-EdgeGraspNet [12]. Following Section 3.5, here we analyze TARGO-Net in detail. Figure 4 reveals that our TARGO-Net drops the least: only about 7%, and is less affected by severe occlusion. TARGO-Net takes the scene and complete target point clouds as inputs and employs cross-attention layers to learn from scene and target features, achieving state-of-the-art performance in the target-driven grasping task against occlusion.

Real-world experiments. We test our TARGO-Net on the real hardware. For the packed scenarios, at least 10 rounds of experiments are performed with GIGA and TARGO-Net at each occlusion level: Easy in $[0, 0.3)$; Medium in $[0.3, 0.6)$; Hard in $[0.6, 0.9)$. In each round, at least 5 objects are randomly selected from 18 test objects and placed on the table, and one target is randomly selected for grasping. In each grasp trial, we feed the back-projected partial point cloud from a side-view depth image to the model and execute the predicted best grasp. A grasp trial is considered successful if the robot grasps the object and places it in a container next to the workspace. Table 2 reports the real-world evaluations. TARGO-Net achieves higher success rates and picks more targets at each

Table 2: Comparison of GIGA and our TARGO-Net over three occlusion levels in the real world.

Methods	Easy [0, 0.3)	Medium [0.3, 0.6)	Hard [0.6, 0.9)
GIGA [15]	70.0	40.0	30.0
TARGO-Net (ours)	80.0	75.0	66.7

occlusion level. However, we still see an overall decline of 14%, whereas the drop in the simulation (as seen in Fig. 4) is only 7%. The discrepancy is due to distinct noise patterns that pose a challenge to shape completion in the real world. Videos of target-driven grasping real-world experiments are available on our website.

5.1 Ablation studies

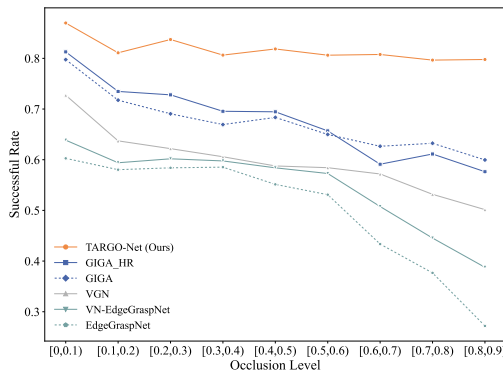


Figure 4: Comparisons of our TARGO-Net and baselines.

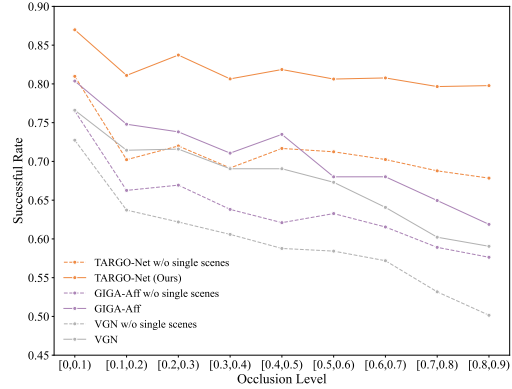


Figure 5: Effects of data augmentation with single scenes.

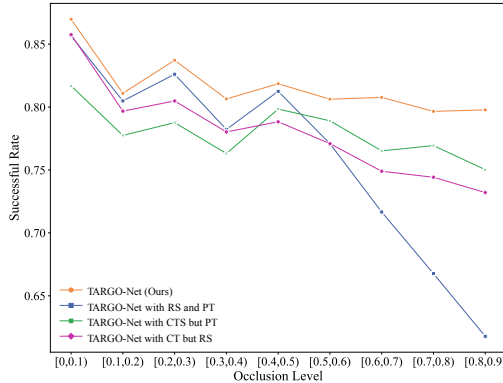


Figure 6: Effects of the input completeness.

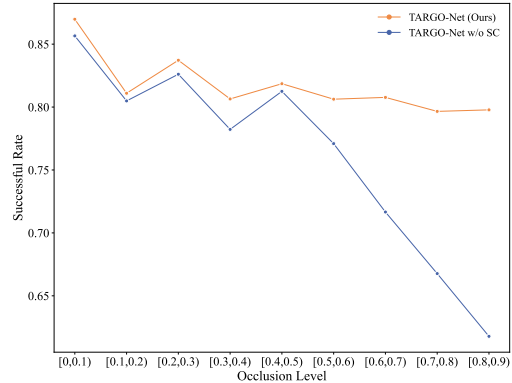


Figure 7: Effects of shape completion.

Data augmentation with single scenes. We train VGN and GIGA-Aff with the VGN dataset (without single scenes) and our TARGO-Net with the TARGO-Synthetic training set to prove the effectiveness of single scenes. As shown in Fig. 5, methods incorporating single scene data augmentation demonstrate a significant advantage over those without them.

Effects of the input completeness. Here we analyze the effect of the completeness of the input point clouds on our TARGO-Net. Note that we complete the Partial Target (PT) through our shape completion module and then define it as the Complete Target (CT), and refer to the Complete Target Scene (CTS) as placing the CT back into the Raw Scene point cloud (RS). Regarding the scene and target object as inputs, we thus have four variants of TARGO-Net: TARGO-Net (Ours, with CTS

Table 3: Quantitative results of target completion evaluated in $CD-\ell_1$ ($\times 1000$) and IoU.

Method	$CD-\ell_1 \downarrow$	IoU (%) \uparrow
GIGA [15]	8.722	78.77
GIGA-Geo [15]	5.588	85.67
TARGO-Net (ours)	2.443	93.99

and CT), TARGO-Net with CTS but PT, TARGO-Net with CT but RS, and TARGO-Net with RS and PT. As shown in 6, TARGO-Net demonstrates relatively high and stable performance across all occlusion levels. In contrast, TARGO-Net with PT and RS exhibits the most significant drop in success rate, decreasing by approximately 20% after the [0.4, 0.5] range. TARGO-Net with CTS but PT shows a decline of about 10% in success rate, while TARGO-Net with CT but RS exhibits a decrease of around 12%. Overall, TARGO-Net proves to be more robust against varying occlusion levels compared to the other configurations, maintaining a success rate close to 85% even at higher occlusion levels.

Effects of shape completion. Fig. 7 signifies that TARGO-Net performs well at low occlusion levels with and without the shape completion module. However, when the occlusion levels increase from 0.4, the performance of TARGO-Net without the shape completion module drops rapidly, up to 18% decrease compared with TARGO-Net.

Shape completion vs. scene completion. GIGA (with both scene completion and affordance prediction) and GIGA-Geo (trained solely for scene completion without the affordance prediction branch) both reconstruct **scene** mesh utilize Convolutional Occupancy Networks [30], while TARGO-Net employs a geometry-aware Transformer to complete partial **target** shape. In Table 3, we see that TARGO-Net surpasses GIGA and GIGA-Geo by a large margin in terms of both Chamfer L1 Distance and Volumetric IoU, subsequently enabling our grasp detection networks to better predict grasps. Further qualitative results can be found in Appendix A.4.

Additional factors influencing target-driven grasping. In addition to occlusion level, we have investigated more possible factors affecting target-driven grasping, such as the *number of occluders*, and the *size of the target object*, which is defined as the minimal length of its length and width of the bounding box. In Fig. 8, we present experiments on TARGO-Synthetic test dataset on occlusion level [0.5, 0.6) to explore how *target object size* influences the success rate of target-driven grasping for both TARGO-Net and GIGA [15].

Using a gripper with a maximum opening width of 0.08 m, we observe that objects with sizes in the range (0.0509, 0.0626] have the highest grasp success rate. For objects larger or smaller than this range, the grasp success rate decreases. This suggests that an appropriate object size facilitates grasping success better, likely due to the common grasping patterns that involve grasping from the sides. This finding provides insight into selecting an appropriate gripper width according to the target object size in future experiments. Please refer to Appendix A.5 for more experiment details about *target object size* and analysis on *number of occluders*.

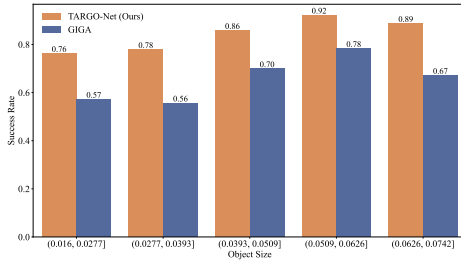


Figure 8: Analysis of factors except for occlusion level that affects grasp success rate. The target object size influences the success rate when it is at the same occlusion level.

6 Conclusion

To the best of our knowledge, this is the first study focusing on target-driven grasping under occlusion in robotics. In this work, we proposed a new synthetic and real-world benchmark dataset for evaluating the robustness of models against occlusion, TARGO, based on VGN and YCB datasets. Our study yields several key findings: 1) *Augmentation with single scenes benefits all models*, 2) *Target as input improves performance*, and 3) *Shape completion is beneficial but does not generalize to real-world*

environments. Additionally, we propose a transformer-based model with a shape-completion module, TARGO-Net, which outperforms existing models on the proposed occluded synthetic and real-world datasets.

References

- [1] Michel Breyer, Jen Jen Chung, Lionel Ott, Roland Siegwart, and Juan Nieto. Volumetric grasping network: Real-time 6 dof grasp detection in clutter. In *Conference on Robot Learning*, pages 1602–1611. PMLR, 2021.
- [2] Berk Calli, Arjun Singh, Aaron Walsman, Siddhartha Srinivasa, Pieter Abbeel, and Aaron M Dollar. The ycb object and model set: Towards common benchmarks for manipulation research. In *2015 international conference on advanced robotics (ICAR)*, pages 510–517. IEEE, 2015.
- [3] Yu-Wei Chao, Wei Yang, Yu Xiang, Pavlo Molchanov, Ankur Handa, Jonathan Tremblay, Yashraj S Narang, Karl Van Wyk, Umar Iqbal, Stan Birchfield, et al. Dexycb: A benchmark for capturing hand grasping of objects. In *Proceedings of the IEEE/CVF Conference on Computer Vision and Pattern Recognition*, pages 9044–9053, 2021.
- [4] Nikhil Chavan-Dafle, Sergiy Popovych, Shubham Agrawal, Daniel D Lee, and Volkan Isler. Simultaneous object reconstruction and grasp prediction using a camera-centric object shell representation. In *2022 IEEE/RSJ International Conference on Intelligent Robots and Systems (IROS)*, pages 1396–1403. IEEE, 2022.
- [5] Sang Hun Cheong, Brian Y Cho, Jinhwi Lee, ChangHwan Kim, and Changjoo Nam. Where to relocate?: Object rearrangement inside cluttered and confined environments for robotic manipulation. In *2020 IEEE International Conference on Robotics and Automation (ICRA)*, pages 7791–7797. IEEE, 2020.
- [6] Woojin Chung, Seokgyu Kim, Minki Choi, Jaesik Choi, Hoyeon Kim, Chang-bae Moon, and Jae-Bok Song. Safe navigation of a mobile robot considering visibility of environment. *IEEE Transactions on Industrial Electronics*, 56(10):3941–3950, 2009.
- [7] Clemens Eppner, Arsalan Mousavian, and Dieter Fox. Acronym: A large-scale grasp dataset based on simulation. In *2021 IEEE International Conference on Robotics and Automation (ICRA)*, pages 6222–6227. IEEE, 2021.
- [8] Hao-Shu Fang, Chenxi Wang, Minghao Gou, and Cewu Lu. Graspnet-1billion: A large-scale benchmark for general object grasping. In *Proceedings of the IEEE/CVF conference on computer vision and pattern recognition*, pages 11444–11453, 2020.
- [9] Shresth Grover, Vibhav Vineet, and Yogesh Rawat. Revealing the unseen: Benchmarking video action recognition under occlusion. *Advances in Neural Information Processing Systems*, 36, 2024.
- [10] Basile Van Hoorick, Pavel Tokmakov, Simon Stent, Jie Li, and Carl Vondrick. Tracking through containers and occluders in the wild, 2023.
- [11] Cheng-Yen Hsieh, Tarasha Khurana, Achal Dave, and Deva Ramanan. Tracking any object amodally. *arXiv preprint arXiv:2312.12433*, 2023.
- [12] Haojie Huang, Dian Wang, Xupeng Zhu, Robin Walters, and Robert Platt. Edge grasp network: A graph-based se (3)-invariant approach to grasp detection. In *2023 IEEE International Conference on Robotics and Automation (ICRA)*, pages 3882–3888. IEEE, 2023.
- [13] Margaret E Jefferies, Jesse Baker, and Wengrong Weng. Robot cognitive mapping—a role for a global metric map in a cognitive mapping process. In *Robotics and cognitive approaches to spatial mapping*, pages 265–279. Springer, 2008.
- [14] Yun Jiang, Stephen Moseson, and Ashutosh Saxena. Efficient grasping from rgb-d images: Learning using a new rectangle representation. In *2011 IEEE International conference on robotics and automation*, pages 3304–3311. IEEE, 2011.
- [15] Zhenyu Jiang, Yifeng Zhu, Maxwell Svetlik, Kuan Fang, and Yuke Zhu. Synergies between affordance and geometry: 6-dof grasp detection via implicit representations. *Robotics: science and systems*, 2021.

- [16] Lei Ke, Yu-Wing Tai, and Chi-Keung Tang. Deep occlusion-aware instance segmentation with overlapping bilayers. In *Proceedings of the IEEE/CVF conference on computer vision and pattern recognition (CVPR)*, pages 4019–4028, 2021.
- [17] Diederik P Kingma and Jimmy Ba. Adam: A method for stochastic optimization. *The 3rd International Conference for Learning Representations*, 2015.
- [18] Alexander Kirillov, Eric Mintun, Nikhila Ravi, Hanzi Mao, Chloe Rolland, Laura Gustafson, Tete Xiao, Spencer Whitehead, Alexander C Berg, Wan-Yen Lo, et al. Segment anything. *arXiv preprint arXiv:2304.02643*, 2023.
- [19] Adam Kortylewski, Ju He, Qing Liu, and Alan L Yuille. Compositional convolutional neural networks: A deep architecture with innate robustness to partial occlusion. In *Proceedings of the IEEE/CVF Conference on Computer Vision and Pattern Recognition*, pages 8940–8949, 2020.
- [20] James J Kuffner. Effective sampling and distance metrics for 3d rigid body path planning. In *IEEE International Conference on Robotics and Automation, 2004. Proceedings. ICRA'04. 2004*, volume 4, pages 3993–3998. IEEE, 2004.
- [21] Andrey Kurenkov, Joseph Taglic, Rohun Kulkarni, Marcus Dominguez-Kuhne, Animesh Garg, Roberto Martín-Martín, and Silvio Savarese. Visuomotor mechanical search: Learning to retrieve target objects in clutter. In *2020 IEEE/RSJ International Conference on Intelligent Robots and Systems (IROS)*, pages 8408–8414. IEEE, 2020.
- [22] Jinhwi Lee, Younggil Cho, Changjoo Nam, Jonghyeon Park, and Changhwan Kim. Efficient obstacle rearrangement for object manipulation tasks in cluttered environments. In *2019 International Conference on Robotics and Automation (ICRA)*, pages 183–189. IEEE, 2019.
- [23] Sergey Levine, Peter Pastor, Alex Krizhevsky, Julian Ibarz, and Deirdre Quillen. Learning hand-eye coordination for robotic grasping with deep learning and large-scale data collection. *The International journal of robotics research*, 37(4-5):421–436, 2018.
- [24] Yu Li, Kai Cheng, Ruihai Wu, Yan Shen, Kaichen Zhou, and Hao Dong. Mobileafford: Mobile robotic manipulation through differentiable affordance learning. In *2nd Workshop on Mobile Manipulation and Embodied Intelligence at ICRA 2024*, 2024.
- [25] Zhan Liu, Ziwei Wang, Sichao Huang, Jie Zhou, and Jiwen Lu. Ge-grasp: Efficient target-oriented grasping in dense clutter. In *2022 IEEE/RSJ International Conference on Intelligent Robots and Systems (IROS)*, pages 1388–1395. IEEE, 2022.
- [26] Daniel Maturana and Sebastian Scherer. Voxnet: A 3d convolutional neural network for real-time object recognition. In *2015 IEEE/RSJ International Conference on Intelligent Robots and Systems (IROS)*, pages 922–928. IEEE, 2015.
- [27] Rajat Modi, Vibhav Vineet, and Yogesh Rawat. On occlusions in video action detection: Benchmark datasets and training recipes. *Advances in Neural Information Processing Systems*, 36, 2023.
- [28] Adithyavairavan Murali, Arsalan Mousavian, Clemens Eppner, Chris Paxton, and Dieter Fox. 6-dof grasping for target-driven object manipulation in clutter. In *2020 IEEE International Conference on Robotics and Automation (ICRA)*, pages 6232–6238. IEEE, 2020.
- [29] Ege Ozguroglu, Ruoshi Liu, Dídac Surís, Dian Chen, Achal Dave, Pavel Tokmakov, and Carl Vondrick. pix2gestalt: Amodal segmentation by synthesizing wholes. *arXiv preprint arXiv:2401.14398*, 2024.
- [30] Songyou Peng, Michael Niemeyer, Lars Mescheder, Marc Pollefeys, and Andreas Geiger. Convolutional occupancy networks. In *Computer Vision—ECCV 2020: 16th European Conference, Glasgow, UK, August 23–28, 2020, Proceedings, Part III 16*, pages 523–540. Springer, 2020.
- [31] Abhishek Sharma, Oliver Grau, and Mario Fritz. Vconv-dae: Deep volumetric shape learning without object labels. In *European Conference on Computer Vision*, pages 236–250. Springer, 2016.
- [32] Maximilian Stölzle, Takahiro Miki, Levin Gerdes, Martin Azkarate, and Marco Hutter. Reconstructing occluded elevation information in terrain maps with self-supervised learning. *IEEE Robotics and Automation Letters*, 7(2):1697–1704, 2022.
- [33] Martin Sundermeyer, Arsalan Mousavian, Rudolph Triebel, and Dieter Fox. Contact-graspnet: Efficient 6-dof grasp generation in cluttered scenes. In *2021 IEEE International Conference on Robotics and Automation (ICRA)*, pages 13438–13444. IEEE, 2021.

- [34] Lyne P Tchammi, Vineet Kosaraju, Hamid Rezaatofighi, Ian Reid, and Silvio Savarese. Topnet: Structural point cloud decoder. In *Proceedings of the IEEE Conference on Computer Vision and Pattern Recognition*, pages 383–392, 2019.
- [35] Angtian Wang, Yihong Sun, Adam Kortylewski, and Alan L Yuille. Robust object detection under occlusion with context-aware compositionalnets. In *Proceedings of the IEEE/CVF Conference on Computer Vision and Pattern Recognition*, pages 12645–12654, 2020.
- [36] Lizi Wang, Hongkai Ye, Qianhao Wang, Yuman Gao, Chao Xu, and Fei Gao. Learning-based 3d occupancy prediction for autonomous navigation in occluded environments. In *2021 IEEE/RSJ International Conference on Intelligent Robots and Systems (IROS)*, pages 4509–4516. IEEE, 2021.
- [37] Ruihai Wu, Chuanruo Ning, and Hao Dong. Learning foresightful dense visual affordance for deformable object manipulation. In *IEEE International Conference on Computer Vision (ICCV)*, 2023.
- [38] Ruihai Wu, Yan Zhao, Kaichun Mo, Zizheng Guo, Yian Wang, Tianhao Wu, Qingnan Fan, Xuelin Chen, Leonidas Guibas, and Hao Dong. VAT-mart: Learning visual action trajectory proposals for manipulating 3d ARTiculated objects. In *International Conference on Learning Representations*, 2022.
- [39] Zhirong Wu, Shuran Song, Aditya Khosla, Fisher Yu, Linguang Zhang, Xiaoou Tang, and Jianxiong Xiao. 3d shapenets: A deep representation for volumetric shapes. In *Proceedings of the IEEE conference on computer vision and pattern recognition*, pages 1912–1920, 2015.
- [40] Yan Xia, Mariia Gladkova, Rui Wang, Qianyun Li, Uwe Stilla, Joao F Henriques, and Daniel Cremers. Casspr: Cross attention single scan place recognition. In *Proceedings of the IEEE/CVF International Conference on Computer Vision*, pages 8461–8472, 2023.
- [41] Yan Xia, Yusheng Xu, Cheng Wang, and Uwe Stilla. Vpc-net: Completion of 3d vehicles from mls point clouds. *ISPRS Journal of Photogrammetry and Remote Sensing*, 174:166–181, 2021.
- [42] Yaqi Xia, Yan Xia, Wei Li, Rui Song, Kailang Cao, and Uwe Stilla. Asfm-net: Asymmetrical siamese feature matching network for point completion. In *Proceedings of the 29th ACM international conference on multimedia*, pages 1938–1947, 2021.
- [43] Katherine Xu, Lingzhi Zhang, and Jianbo Shi. Amodal completion via progressive mixed context diffusion. *arXiv preprint arXiv:2312.15540*, 2023.
- [44] Yang Yang, Hengyue Liang, and Changhyun Choi. A deep learning approach to grasping the invisible. *IEEE Robotics and Automation Letters*, 5(2):2232–2239, 2020.
- [45] Xumin Yu, Yongming Rao, Ziyi Wang, Jiwen Lu, and Jie Zhou. Adapointr: Diverse point cloud completion with adaptive geometry-aware transformers. *IEEE Transactions on Pattern Analysis and Machine Intelligence*, 2023.
- [46] Wentao Yuan, Tejas Khot, David Held, Christoph Mertz, and Martial Hebert. Pcn: Point completion network. In *2018 International Conference on 3D Vision (3DV)*, pages 728–737. IEEE, 2018.
- [47] Xiaoding Yuan, Adam Kortylewski, Yihong Sun, and Alan Yuille. Robust instance segmentation through reasoning about multi-object occlusion. In *Proceedings of the IEEE/CVF Conference on Computer Vision and Pattern Recognition*, pages 11141–11150, 2021.
- [48] Andy Zeng, Shuran Song, Kuan-Ting Yu, Elliott Donlon, Francois R Hogan, Maria Bauza, Daolin Ma, Orion Taylor, Melody Liu, Eudald Romo, et al. Robotic pick-and-place of novel objects in clutter with multi-affordance grasping and cross-domain image matching. *The International Journal of Robotics Research*, 41(7):690–705, 2022.
- [49] Guanqi Zhan, Weidi Xie, and Andrew Zisserman. A tri-layer plugin to improve occluded detection. *British Machine Vision Conference (BMVC)*, 2022.
- [50] Guanqi Zhan, Chuanxia Zheng, Weidi Xie, and Andrew Zisserman. Amodal ground truth and completion in the wild. *The IEEE Conference on Computer Vision and Pattern Recognition (CVPR)*, 2024.
- [51] Xiaohang Zhan, Xingang Pan, Bo Dai, Ziwei Liu, Dahua Lin, and Chen Change Loy. Self-supervised scene de-occlusion. In *Proceedings of the IEEE/CVF Conference on Computer Vision and Pattern Recognition (CVPR)*, pages 3784–3792, 2020.

- [52] Kaichen Zhou, Lanqing Hong, Changhao Chen, Hang Xu, Chaoqiang Ye, Qingyong Hu, and Zhenguo Li. Devnet: Self-supervised monocular depth learning via density volume construction. In *European Conference on Computer Vision*, pages 125–142. Springer, 2022.
- [53] Kaichen Zhou, Jia-Xing Zhong, Sangyun Shin, Kai Lu, Yiyuan Yang, Andrew Markham, and Niki Trigoni. Dynpoint: Dynamic neural point for view synthesis. *Advances in Neural Information Processing Systems*, 36, 2024.
- [54] Yan Zhu, Yuandong Tian, Dimitris Metaxas, and Piotr Dollár. Semantic amodal segmentation. In *Proceedings of the IEEE Conference on Computer Vision and Pattern Recognition (CVPR)*, pages 1464–1472, 2017.
- [55] René Zurbrügg, Yifan Liu, Francis Engelmann, Suryansh Kumar, Marco Hutter, Vaishakh Patil, and Fisher Yu. Icgnet: A unified approach for instance-centric grasping. *arXiv preprint arXiv:2401.09939*, 2024.

A Appendix

A.1 Overview

All benchmark datasets and the associated code are accessible to the public via <https://TARGO-benchmark.github.io/>. We offer more experiments, analyses, and insights obtained throughout the development in this appendix.

A.2 License

We utilize the standard CC BY-NC 4.0 licenses from the community and offer the following links to the non-commercial licenses for the datasets used in this paper.

VGN [1]: <https://github.com/ethz-asl/vgn/blob/cor12020/LICENSE>

DexYCB [3]: <https://creativecommons.org/licenses/by-nc/4.0/>

A.3 Dataset

This section details generating our cluttered and single scenes in our TARGO dataset. We first explain why only packed scenes are used in our grasping datasets and then introduce why the single scenes can help the grasping success rates.

Reason for using only packed scenes in TARGO. As defined in [1], the *pile* configuration randomly drops objects into a box of the same size as the workspace. When the box is removed, a cluttered pile of objects remains. In the *packed* configuration, a subset of the pile objects are placed at random positions on the table in their canonical poses. Fig. 9 visualizes examples of both configurations. Note that we intentionally exclude the pile setup for single scenes. In the pile setup, if an object (e.g., a red bowl) sits on top of another object (e.g., a Pepsi caffeine box), removing the object at the bottom will cause the top object to fall onto the table, changing its pose. Since we require the same object pose in the cluttered scene to construct a corresponding single scene, we focus only on packed scenes in our dataset.

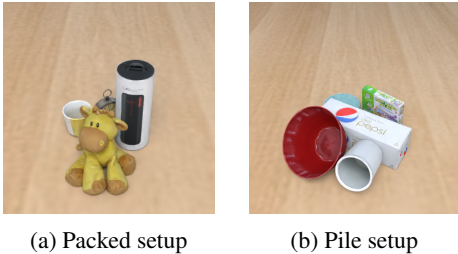


Figure 9: Packed and pile scenarios.

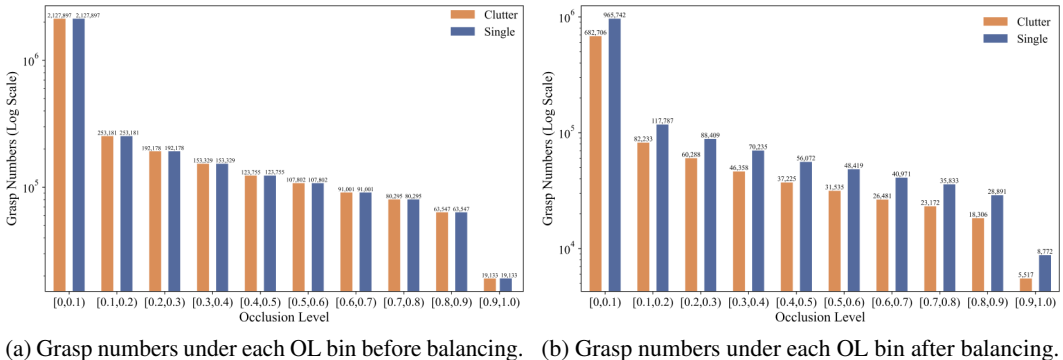


Figure 10: Comparison of unbalanced and balanced grasps numbers in single and cluttered scenes under different occlusion levels.

Analysis of Single Scenes. Empirical observations show that in cluttered scenes, the number of negative grasps significantly outnumbers the positive ones. Fortunately, this can be addressed by incorporating single scenes. Initially, both cluttered and single scenes share the same set of planned

grasps for each occlusion level (as illustrated in Fig. 10a). However, because the positive grasps in cluttered scenes are a subset of those in single scenes, more positive grasps from single scenes remain after balancing (as shown in Fig. 10b). Thus, incorporating single scenes allows us to achieve a higher number of positive grasps with the same number of grasp trials, thereby improving the efficiency of our grasp sampling process and the grasping robustness of our TARGO-Net.

A.4 Additional Ablation Studies of TARGO-Net

Following Section 5.1 in the main paper, we further compare the performance of our Transformer backbone with that of a CNN backbone. Then, we study the impact of using different numbers of Transformer layers in our TARGO-Net. Finally, we compare the performance of shape completion and scene completion and analyze the effects of shape completion in our target-driven grasping task.

Transformer vs. CNN backbone. To compare Transformer and CNN backbones fairly, we exclude shape completion and compare TARGO-Net w/o SC (without shape completion) and GIGA-Aff (an ablated version of GIGA trained solely for affordance prediction without the scene completion branch) models with single scene augmentation. In all models, we input both the partial scene and partial target. TARGO-Net w/o SC employs a Cross-Attention Transformer (CAT) [40] to process the input and uses concatenation to fuse the features. In contrast, the CNN_Concat and CNN_Add models use 3D CNNs in GIGA-Aff to process the input and employ concatenation and addition to fuse the feature grids, respectively. We used the TARGO-Synthetic test dataset with Gaussian noise with a mean of 0 and standard deviations (σ) of 0.002, the same as the training setting, and 0.005 to test model robustness. As shown in Fig. 11, TARGO-Net w/o SC generally performs best for most occlusion levels. With more severe Gaussian noise ($\sigma = 0.005$), TARGO-Net w/o SC is, on average 2% better than the second best model and 5% better than the worst model in these bins. With Gaussian noise ($\sigma = 0.002$), TARGO-Net w/o SC has a slightly less pronounced advantage over the CNN-based models.

Number of Cross-Attention Transformer layers. Here, we investigate the optimal number of Cross-Attention Transformer [40] layers in our TARGO-Net. We separately trained our models with one, two, and three cross-attention layers and tested them using our TARGO-Synthetic test. Fig. 12 shows our model with two Transformer layers performs best. This may be because two layers strike a balance between model complexity and the ability to capture essential features without overfitting, whereas one layer might be too simplistic and three layers might introduce unnecessary complexity.

Shape completion vs. Scene completion. In Fig. 13, we compare the target completion performance of TARGO-Net with GIGA-Geo (trained solely for scene completion without the affordance prediction branch) and GIGA (with both scene completion and affordance prediction). TARGO-Net shows better completion performance than GIGA-Geo and GIGA, which is consistent with the quantitative results in Table 3 of the main paper. For the completion of cuboid and hexagonal prism targets, TARGO-Net achieves near-perfect results, whereas GIGA-Geo and GIGA hardly preserve the shape. In the case of cylinder reconstruction, TARGO-Net loses some details on the top but to a much lesser extent than GIGA-Geo. GIGA, however, predicts a target shape connected with other occluders since it takes all scene voxels as input and occasionally fails to separate occluders near the target. These findings suggest that shape completion approach used by our TARGO-Net is more effective than widely used scene completion approaches for the target-driven grasping task.

Effects of shape completion in TARGO-Net. To investigate the effects of shape completion for target-driven grasping, we qualitatively compare the grasp and affordance predictions between our TARGO-Net and an ablated version, TARGO-Net w/o SC, which reduces the shape completion module. In Fig. 14, the red region in the input view indicates the target object, while in the second and third rows, it represents the grasp affordance predictions. We categorize the comparisons into three occlusion levels, each containing two examples: easy (occlusion range $[0, 0.3)$), middle (occlusion range $[0.3, 0.7)$), and hard (occlusion range $[0.7, 1)$). As illustrated in Fig. 14, the affordance predictions in TARGO-Net w/o SC are limited to the visible input view. In contrast, TARGO-Net’s affordance predictions extend beyond the visible input view, predicting potential grasps in occluded regions. In the easy occlusion level, both methods predict a large affordance region. However, in the medium and hard occlusion levels, TARGO-Net predicts significantly larger high-affordance areas than TARGO-Net w/o SC, as some potential affordance areas are occluded in the input view.

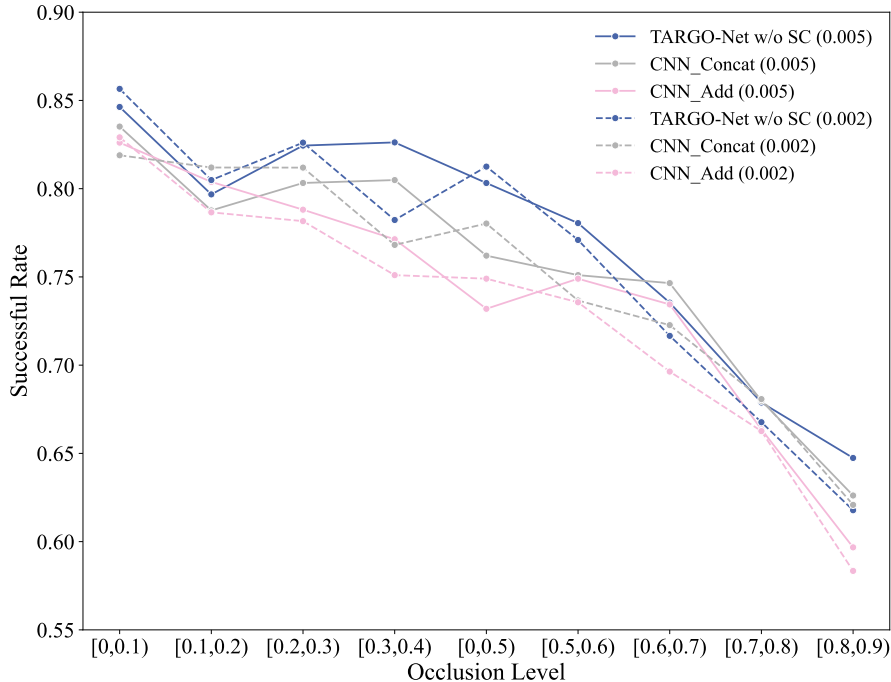


Figure 11: Comparisons of Transformer and CNN backbones without shape/scene completion.

A.5 Additional Factors Influencing GSR

Following analysis in Fig. 8, here we continue exploring two additional factors that may influence the success rate of target-driven grasping: *the number of occluders* (the count of objects blocking the view of the target) and *the target object’s size* (defined as the minimum length and width of the bounding box surrounding the target object). To isolate the impact of occlusion level, we select three subsets from TARGO-Synthetic test dataset, each with a different occlusion range: $[0.2, 0.3)$, $[0.5, 0.6)$, and $[0.7, 0.8)$. Each subset contains 1000 test samples. We used TARGO-Net and GIGA to evaluate and analyze the success rates across these subsets.

Number of occluders. In Fig. 15, we analyze the grasp success rate (GSR) of TARGO-Net and GIGA as the number of occluders increases from 2 to 6 across three occlusion ranges. In the occlusion range $[0.2, 0.3)$, TARGO-Net’s success rate increases by 14%, whereas GIGA’s success rate decreases by 13%. In the range $[0.5, 0.6)$, TARGO-Net shows a 3% increase, while GIGA shows a 9% decrease. In the range $[0.7, 0.8)$, TARGO-Net experiences a 3% decrease, while GIGA’s success rate decreases by 15%. Overall, TARGO-Net demonstrates relatively stable performance with minor fluctuations across different numbers of occluders. In contrast, GIGA exhibits more significant variability, particularly with noticeable drops in success rate at higher occlusion levels.

Target object size. As shown in Fig. 16, in both GIGA and TARGO-Net, across all three occlusion ranges, objects with sizes in the range of $(0.0509, 0.0626]$ have the highest grasp success rates. For objects larger or smaller than this range, the success rate decreases. This suggests that an appropriate object size facilitates better grasping. In addition, TARGO-Net performs more stably than GIGA when encountering different target object sizes.

A.6 Additional Results on TARGO-Real Dataset

In this section, we test the grasp performance on the TARGO-Real dataset for TARGO-Net and five baselines, including GIGA [15], GIGA-HR [15], VGN [1], EdgeGraspNet [12], and VN-EdgeGraspNet [12]. Note that all methods are trained on the TARGO-Synthetic training dataset. Fig. 17 shows that the performance of all methods drops sharply compared to their performance in the TARGO-Synthetic test dataset. The results are consistent with expectations due to the domain

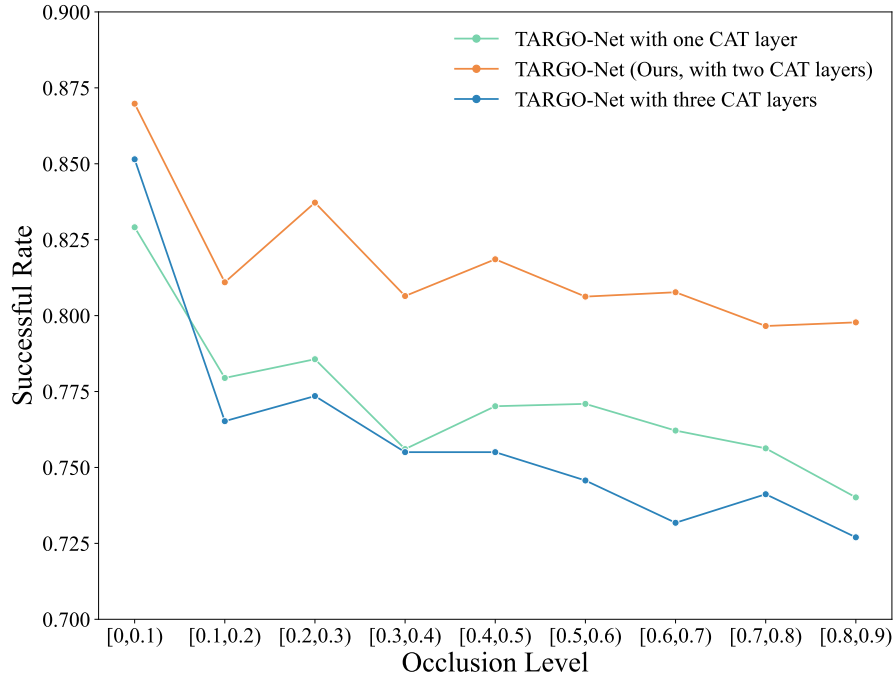


Figure 12: Grasp performance for TARGO-Net with different numbers of CAT layers.

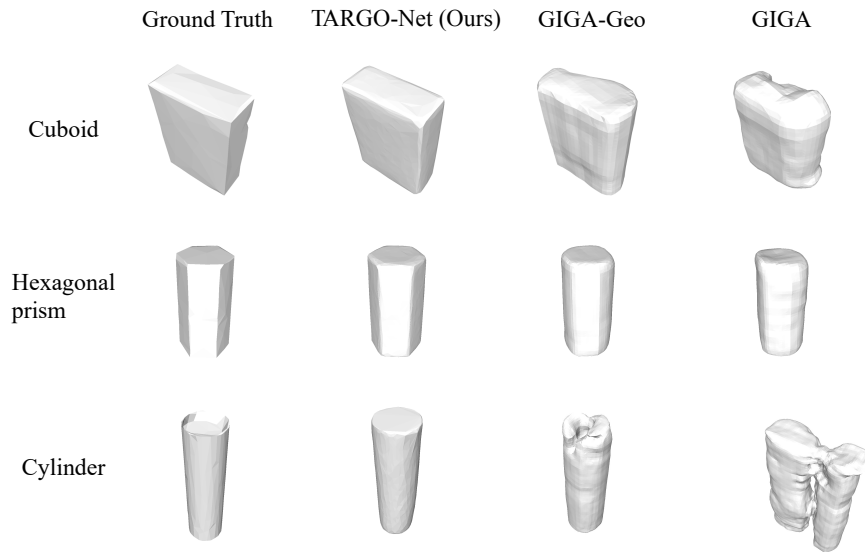


Figure 13: Qualitative target completion comparisons using our shape and scene completion in GIGA.

differences in objects and their arrangements between the real-world and synthetic training data. Another possible reason is that we changed the workstation size from $0.3 \text{ m} \times 0.3 \text{ m} \times 0.3 \text{ m}$ in the simulation environment to $0.7 \text{ m} \times 0.7 \text{ m} \times 0.7 \text{ m}$ in real-world grasping, causing more challenges.

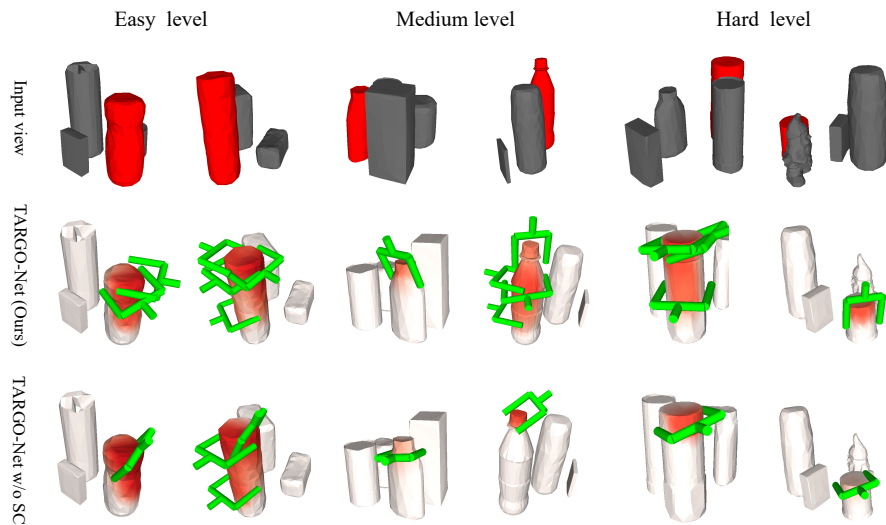


Figure 14: Effects of the shape completion on TARGO-Synthetic dataset. 'w/o SC' indicates removing the proposed shape completion in TARGO-Net.

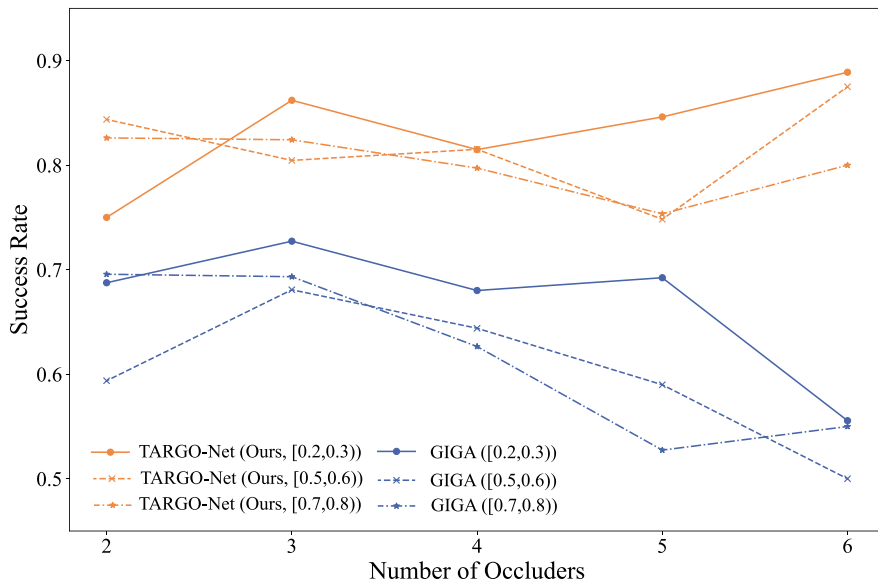


Figure 15: Grasp performance with different numbers of occluders on TARGO-Synthetic dataset.

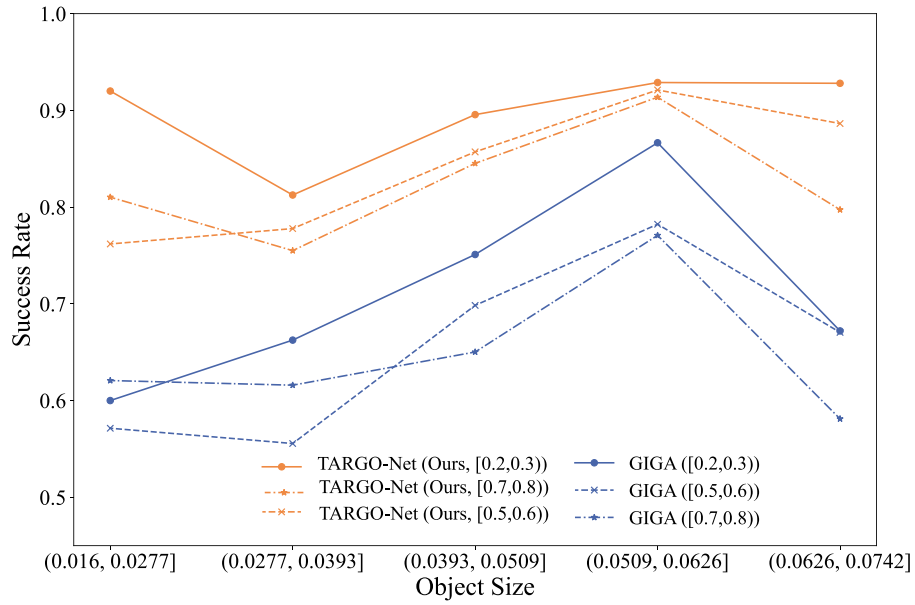


Figure 16: Grasp performance with different object sizes on TARGO-Synthetic dataset.

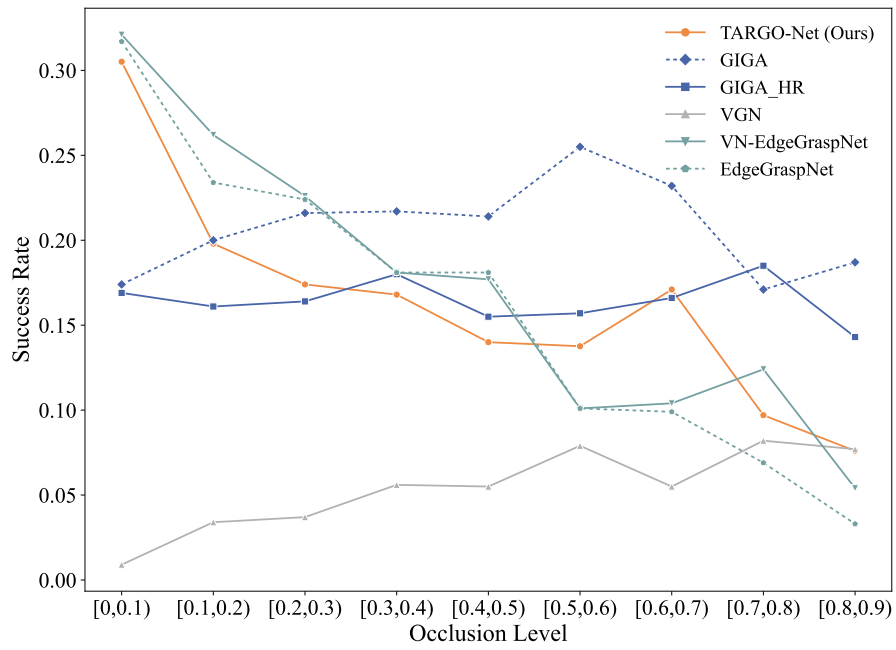


Figure 17: Comparisons of TARGO-Net with other baselines on TARGO-Real dataset.